



Fermi National Accelerator Laboratory

FERMILAB-Pub-92/141-E

E705

# A Measurement of $J/\Psi$ and $\psi'$ Production in 300 GeV/c Proton, Antiproton and $\pi^\pm$ Nucleon Interactions

E705

*Fermi National Accelerator Laboratory  
P.O. Box 500, Batavia, Illinois 60510*

May 1992

Submitted to *Physics Review D*

## **Disclaimer**

*This report was prepared as an account of work sponsored by an agency of the United States Government. Neither the United States Government nor any agency thereof, nor any of their employees, makes any warranty, express or implied, or assumes any legal liability or responsibility for the accuracy, completeness, or usefulness of any information, apparatus, product, or process disclosed, or represents that its use would not infringe privately owned rights. Reference herein to any specific commercial product, process, or service by trade name, trademark, manufacturer, or otherwise, does not necessarily constitute or imply its endorsement, recommendation, or favoring by the United States Government or any agency thereof. The views and opinions of authors expressed herein do not necessarily state or reflect those of the United States Government or any agency thereof.*

A Measurement of  $J/\psi$  and  $\psi'$  Production  
in 300 GeV/c Proton, Antiproton and  $\pi^\pm$  Interactions with Nuclei

The E705 Collaboration

L. Antoniazzi<sup>3</sup>, M. Arenton<sup>9</sup>, Z. Cao<sup>8</sup>, T. Chen<sup>5</sup>, S. Conetti<sup>4</sup>, B. Cox<sup>9</sup>, S. Delchamps<sup>3</sup>,  
L. Fortney<sup>2</sup>, K. Guffey<sup>7</sup>, M. Haire<sup>4</sup>, P. Ioannou<sup>1</sup>, C.M. Jenkins<sup>3</sup>, D.J. Judd<sup>7</sup>,  
C. Kourkouvelis<sup>1</sup>, A. Manousakis-Katsikakis<sup>1</sup>, J. Kuzminski<sup>4</sup>, T. LeCompte<sup>6</sup>,  
A. Marchionni<sup>4</sup>, M. He<sup>8</sup>, P. O. Mazur<sup>3</sup>, C. T. Murphy<sup>3</sup>, P. Pramantiotis<sup>1</sup>,  
R. Rameika<sup>3</sup>, L. K. Resvanis<sup>1</sup>, M. Rosati<sup>4</sup>, J. Rosen<sup>6</sup>, C. Shen<sup>8</sup>, Q. Shen<sup>2</sup>,  
A. Simard<sup>4</sup>, R. P. Smith<sup>3</sup>, L. Spiegel<sup>3</sup>, D. G. Stairs<sup>4</sup>, Y. Tan<sup>6</sup>, R. J. Tesarek<sup>2</sup>,  
T. Turkington<sup>2</sup>, L. Turnbull<sup>7</sup>, F. Turkot<sup>3</sup>, S. Tzamarias<sup>6</sup>, G. Voulgaris<sup>1</sup>,  
D. E. Wagoner<sup>7</sup>, C. Wang<sup>8</sup>, W. Yang<sup>3</sup>, N. Yao<sup>5</sup>, N. Zhang<sup>8</sup>, X. Zhang<sup>8</sup>,  
G. Zioulas<sup>4</sup>, B. Zou<sup>2</sup>

(1) University of Athens, Athens, Greece

(2) Duke University, Durham, NC 27706

(3) Fermi National Accelerator Laboratory, Batavia, IL 60510

(4) McGill University, Montreal, PQ, Canada H3A 2T8

(5) Nanjing University, Nanjing, People's Republic of China

(6) Northwestern University, Evanston, IL 60208

(7) Prairie View A&M University, Prairie View, TX 77445

(8) Shandong University, Jinan, Shandong, People's Republic of China

(9) University of Virginia, Charlottesville, VA 22901

Hadroproduction of the  $J/\psi$  and  $\psi'$  states has been studied in 300 GeV/c proton, antiproton and  $\pi^\pm$  Li interactions. Both total and differential cross sections in  $x_F$  and  $p_T$  have been measured for the  $J/\psi$  for the  $\pi^\pm$ , proton and antiproton interactions. The ratio of  $\psi'$  to  $J/\psi$  production has been determined for the four types of beam particles.

PACS numbers: 13.40.H

The production of charmonium states in hadronic interactions has been a topic of interest for some time because of the insights afforded by these processes into the interactions of quarks and gluons and into the constituent composition of the interacting hadrons. The  $J^{PC}=1^{--}$   $J/\psi$  and  $\psi'$  states have been detected via their dimuon decays in the 300 GeV/c reactions

$$\begin{aligned} p, \bar{p} \text{ or } \pi^\pm \text{ Li} &\longrightarrow J/\psi + \text{anything} \\ &\longrightarrow \mu^+ \mu^- \\ &\text{and} \\ p, \bar{p} \text{ or } \pi^\pm \text{ Li} &\longrightarrow \psi' + \text{anything} \\ &\longrightarrow \mu^+ \mu^- \end{aligned}$$

in an experiment (E705) done in the High Intensity Laboratory (HIL) of the Fermi National Accelerator Laboratory. Both total and differential cross sections have been measured for the inclusive production of  $J/\psi$  and  $\psi'$ .

The 300 GeV/c proton, antiproton and  $\pi^\pm$  beams used in this experiment were a mixture of secondary and tertiary beams produced by 800 GeV/c protons incident on a 40 cm ( $\approx$  one interaction length) Be target. Neutral and charged beams were formed by a magnet/collimator system positioned just downstream of the Be target as shown in Fig. 1. The large acceptance beamline also shown in Fig. 1 transported the charged particles exiting the collimator to the HIL experimental area. The flux captured by this transport was a mixture of 300 GeV/c particles directly produced in the target (secondary flux) and particles from decay of neutrals in the region just downstream of the target (tertiary flux from  $\bar{\Lambda}^0 \rightarrow \bar{p} \pi$ ,  $K_S^0 \rightarrow \pi\pi$  decay). Depending on the availability of primary protons and on whether a positive ( $\pi^+$ , proton) or a negative ( $\pi^-$ , antiproton) beam was desired, the tune of the beamline was varied from one consisting of predominantly secondary flux to one mostly composed of tertiary decay products in order to optimize the antiproton component of the beam. An antiproton composition as large as 8% could be obtained in the tertiary beam mode. Because of the limited flux of 800 GeV/c protons available during the majority of the experiment, the "standard" tune necessary to saturate the data taking capability of the E705 spectrometer was typically close to the charged secondary beam tune and resulted in a 45%  $\pi^+$  and 55% proton mixture for the positive beam and 98%  $\pi^-$  and 2% antiproton for the negative beam. A charged K contamination of less than 6% of the total beam flux was present in both the positive and negative beams.

The typical beam intensity at which the experiment was operated varied during the run from  $1 \times 10^6$  to  $> 5 \times 10^6$  particles per second during the 23 seconds of spill which the experiment received over a 56 second cycle. The beam spill delivered to the experiment had a time structure consisting of 2 ns beam bunches every 18.7 ns during the 23 seconds of spill.

Beam particles were identified as proton, antiproton or  $\pi^\pm$  on a particle by particle basis by

two He beam Cerenkov counters, C1 and C2, operated in the threshold mode. The thresholds of both beam Cerenkov counters were set to produce a signal for a pion and no signal for a proton or an antiproton. To minimize the tagging losses caused by inefficiencies of the Cerenkov counters, the identification of a pion required that either C1 or C2 produced a signal. Correspondingly, to minimize contamination of our antiproton or proton sample, the  $p$  and  $\bar{p}$  were defined by the absence of a signal in both C1 and C2. In addition, the beam definition required a triple coincidence of three stations of scintillation counter hodoscopes. If more than two elements of any one of the three beam hodoscopes were on during any RF bucket, that beam bunch was vetoed.

The number of beam particles of each type that could produce an interaction in the target was recorded for each spill and then corrected for live time, Cerenkov inefficiencies, and multiple bucket occupancy. Uncertainties were determined in two ways: by propagating the measured beam counting and Cerenkov tagging uncertainties through to the final determination of integrated beam flux and by measuring the variation of the interaction/beam flux ratios over the experiment. Both of these methods yielded the same uncertainties in the integrated beam flux for the four beam types and resulted in the following integrated beam totals of  $2.23 \pm 0.11 \times 10^{12} \pi^-$ ,  $1.05 \pm 0.06 \times 10^{12} \pi^+$ ,  $1.29 \pm 0.07 \times 10^{12}$  protons, and  $0.096 \pm 0.003 \times 10^{12}$  antiprotons. These totals have been corrected for dead time, Cerenkov inefficiencies, and multiple bucket occupancy.

The large aperture, open geometry spectrometer<sup>1</sup> used in this experiment is shown in Fig. 2. The spectrometer target was a 33 cm long (0.21 radiation lengths; 0.24 and 0.175 interaction lengths for protons and pions respectively), 5 cm radius cylinder of natural Li (composition: 93%  $^7\text{Li}$ , 7%  $^6\text{Li}$ ). The charged secondaries from the proton, antiproton and  $\pi^\pm\text{Li}$  interactions were measured in a set of PWC and drift chambers positioned upstream and downstream of the spectrometer analysis magnet. The PWC's were deadened in the vicinity of the beam, a region which corresponded approximately to charged tracks with angles less than 25 mradians. The 3'x6' aperture analysis magnet provided a  $p_t$  deflection of 0.776 GeV/c.

An electromagnetic calorimeter<sup>2</sup> and a muon detector were positioned downstream of the last drift chamber. Muons were identified as particles which penetrated both the material of the EM detector and the muon detector (0.40 meters of Cu, 3.7 meters of steel and 0.91 meters of shielding concrete) producing a triple coincidence between elements of three banks of scintillation counters positioned at various depths in the steel. The muon detector imposed a lower bound on the muon momentum of approximately 6 GeV/c for a muon which could satisfy the trigger.

A very important aspect of the spectrometer was the dimuon trigger which consisted of two levels. The first level required that two or more muon triple coincidences be present in different quadrants in a given event. The second level consisted of a trigger processor<sup>3</sup> which processed hits from drift chambers downstream of the spectrometer analysis magnet to find tracks pointing at the muon counter triple coincidences. These tracks were used to form a crude dimuon mass under the

assumption that each track originated in the target. All events passing a mass cut of  $2.4 \text{ GeV}/c^2$  were written to tape. The suppression of the total cross section by this trigger system was approximately a factor of  $3 \times 10^{-4}$ . More than 140 million dimuon triggers (predominantly due to coincidences between muonic decays of charged pions and kaons from the interactions or halo muons that missed the halo veto walls) were accumulated at interaction rates of up to 1.5 MHz.

The 140 million triggers that pass the various trigger levels were subjected to three level of off-line analysis. The first level consisted of a fast filter program which performed a fast reconstruction of the dimuon tracks using only information from detectors downstream of the analysis magnet. A cut at  $2.5 \text{ GeV}/c^2$  was performed on a crude dimuon mass formed from the combination of the bend plane projection tracks and an estimate of the  $y$  slope obtained from a plane of muon scintillation counters oriented parallel to the bend plane. A rejection of approximately 5.5 was achieved with a retention of 98% of the  $J/\psi$ 's. The  $2.5 \times 10^7$  events that passed the filter were subjected to a second stage of analysis in which a full reconstruction of the dimuon tracks was performed. Applying a cut of  $2.6 \text{ GeV}/c^2$  to the dimuon mass spectrum formed using these fully reconstructed muons and demanding opposite sign dimuons cut the data sample to approximately  $10^6$  events while retaining 90% of the  $J/\psi$ 's. A final pass through the remaining data applying tighter cuts on muon track quality, agreement of muon trajectory with muon detector scintillation hodoscope triple coincidences and agreement of slopes and intercepts of track segments formed upstream and downstream of the analysis magnet reduced the data sample to the  $10^5$  dimuons, the mass spectrum of which shown in Fig. 3. Approximately 85% of the signal was retained in this final analysis step.

The four dimuon mass spectra extracted from  $300 \text{ GeV}/c$   $p^\pm N$  and  $\pi^\pm N$  interactions and displayed in Fig. 3 show both  $J/\psi$  and  $\psi'$  peaks. The observed mass resolution ( $\sigma \approx 47 \text{ MeV}/c^2$  where  $\sigma$  is defined as the full width at half maximum divided by 2.36) is consistent with the expected dimuon mass resolution of the spectrometer ( $\sigma \approx 44 \text{ MeV}/c^2$ ) calculated by superimposing Monte Carlo  $J/\psi$  on real events. The signal to background ratio for the various  $J/\psi$  peaks, obtained from a choice of cuts in the reconstruction software, is approximately 3.5 to 4.3 to 1 depending on the choice of mass region for the  $J/\psi$ . For mass region from 2.980 to 3.280  $\text{GeV}/c^2$  (chosen to maximize the number of  $J/\psi$  available for the search for higher mass resonances decaying into  $J/\psi$ ), the  $J/\psi$  to background ratio is 3.5/1. For purposes of the  $x_F$  and  $p_T$  cross section determination, the ratio of the mass of each dimuon pair to the accepted central mass value of  $3097 \text{ MeV}/c^2$  of the  $J/\psi$  was used to rescale the momentum of both muons in order to obtain the best values of the various kinematic quantities.

Correcting for acceptances and efficiencies and subtracting backgrounds (obtained from fits to the dimuon mass regions above and below the  $J/\psi$ ), the total cross sections for production of  $J/\psi$  by the four beam types have been determined (Table I). The errors quoted on the cross sections

are those due to statistics, systematics, and uncertainties of the branching ratios respectively. The systematic error includes contributions due to beam flux counting systematics (9.5%), muon counter efficiency determinations (1.8%), uncertainties in acceptances due to uncertainties in kinematic distributions (0.6%), and Monte Carlo statistics (0.6%). The cross sections per nucleon are calculated from the Li cross sections assuming an atomic weight dependence of the total cross section for  $J/\psi$  production of  $A^{0.92 \pm 0.008}$ . The branching ratio for  $J/\psi \rightarrow \mu^+\mu^-$  used to extract the  $J/\psi$  cross sections is  $0.0591 \pm 0.0011 \pm 0.0020$  as measured by the MARK III collaboration<sup>4</sup>.

Table I  
 $\psi$  Total Cross Sections ( $x_F > 0$ )

Beam Type	$B(\psi \rightarrow \mu\mu) \cdot \sigma/\text{nucleus}$	$\sigma/\text{nucleus (nb)}$	$B(\psi \rightarrow \mu\mu) \cdot \sigma/\text{nucleon}$	$\sigma/\text{nucleon (nb)}$
$\pi^-$	$63.7 \pm 2.1 \pm 6.9$	$1080 \pm 40 \pm 120 \pm 40$	$10.5 \pm 0.3 \pm 1.1$	$182 \pm 7 \pm 20 \pm 7$
$\pi^+$	$62.5 \pm 2.1 \pm 5.2$	$1060 \pm 40 \pm 90 \pm 40$	$10.3 \pm 0.3 \pm 0.9$	$179 \pm 7 \pm 15 \pm 7$
proton	$50.4 \pm 1.6 \pm 5.3$	$850 \pm 30 \pm 90 \pm 30$	$8.4 \pm 0.3 \pm 0.8$	$143 \pm 5 \pm 15 \pm 5$
antiproton	$48.2 \pm 6.7 \pm 4.2$	$820 \pm 110 \pm 70 \pm 30$	$8.1 \pm 1.1 \pm 0.7$	$138 \pm 19 \pm 12 \pm 5$

In Fig. 4a, b, c and d we compare our measurements of the  $BR \cdot \sigma$  for  $J/\psi$  production to those of other experiments<sup>5</sup> at different  $\sqrt{\tau} = M_{\psi}/\sqrt{s}$ . The solid curve shows an empirical parameterization by Lyons<sup>6</sup>. The ratio of the cross sections  $\sigma(\pi^+N \rightarrow J/\psi + x)/\sigma(pN \rightarrow J/\psi + x)$ , which is better determined than the individual cross sections because some of the systematic errors cancel, has been determined to be  $1.246 \pm 0.034 \pm 0.022$  for the positive beam production of  $J/\psi$ . The ratio  $\sigma(\pi^-N \rightarrow J/\psi + x)/\sigma(\bar{p}N \rightarrow J/\psi + x)$  is dominated by statistical errors.

The ratio  $BR(\psi' \rightarrow \mu\mu) \cdot \sigma(xN \rightarrow \psi' + x)/BR(J/\psi \rightarrow \mu\mu) \cdot \sigma(xN \rightarrow J/\psi + x)$  has been determined for the four beam types from the data of Fig. 3. The values of those ratios for the four different beam types together with the ratio  $\sigma(xN \rightarrow \psi' + x)/\sigma(xN \rightarrow J/\psi + x)$  obtained using the MARK III measurement of the  $J/\psi \rightarrow \mu^+\mu^-$  branching ratio,  $0.0591 \pm 0.011 \pm 0.020$ , and the weighted average of the  $\psi' \rightarrow \mu^+\mu^-$  and  $\psi' \rightarrow e^+e^-$  branching ratios,  $0.0082 \pm 0.0011$ , are shown in Table II below:

Table II  
 $BR(\psi' \rightarrow \mu\mu) \cdot \sigma(\psi')/BR(J/\psi \rightarrow \mu\mu) \cdot \sigma(J/\psi)$  and  $\sigma(\psi')/\sigma(J/\psi)$   
for 300 GeV/c  $\pi^\pm N$  and  $p^\pm N$  Interactions

Beam	$BR \cdot \sigma(\psi')/BR \cdot \sigma(J/\psi)$	$\sigma(\psi')/\sigma(J/\psi)$
$\pi^+$	$0.0166 \pm 0.0044 \pm 0.0004$	$0.12 \pm 0.03 \pm 0.003 \pm 0.02$
$\pi^-$	$0.0193 \pm 0.0026 \pm 0.0005$	$0.14 \pm 0.02 \pm 0.004 \pm 0.02$
proton	$0.0188 \pm 0.0026 \pm 0.0005$	$0.14 \pm 0.02 \pm 0.004 \pm 0.02$
antiproton	$0.0348 \pm 0.0304 \pm 0.0010$	$0.25 \pm 0.22 \pm 0.007 \pm 0.04$

In Fig. 5a, b, c and d we compare our measurements of the ratio of  $BR \cdot \sigma$  for  $\Psi'$  to  $BR \cdot \sigma$  for  $J/\Psi$  to those of other experiments<sup>7</sup> at different  $\sqrt{\tau} = M_{\Psi'} / \sqrt{s}$ .

The differential cross sections  $d\sigma/dx_F$  for  $J/\Psi$  production are shown in Fig. 6a, b, c and d for  $\pi^+$ ,  $\pi^-$ , proton and antiproton data and the cross sections and their statistical errors are given in Table III.

Table III  
 $d\sigma/dx_F$  Differential Cross Sections

$x_F$	$\pi^-$ (nb)	$\pi^+$ (nb)	Proton (nb)	Antiproton
- 0.10	416±89	269±88	445±94	
- 0.05	513±55	436±58	531±71	
0.00	472±28	503±39	645±40	547±328
0.05	473±22	492±28	597±30	
0.10	463±14	464±20	514±22	485±142
0.15	397±11	459±18	438±16	
0.20	372±11	365±21	330±19	340±83
0.25	333±13	329±22	238±15	
0.30	294±15	284±21	169±21	251±77
0.35	258±30	301±93	108±24	
0.40	178±34	188±45	57±18	129±92
0.45	89±26	85±89	25±11	

The bin width is 0.05 for the  $\pi^\pm$  and proton data and 0.10 for the antiproton data. The high  $x_F$  region for forward  $J/\Psi$  production was difficult to measure in this experiment because of the deadening of the PWC's in beam region (corresponding to muon angles less than 25 mradians) and the confusion near the beam region caused by overlapping tracks and rate effects due to pileup at high intensities. In order to take these effects into account, the efficiency for extracting  $J/\Psi$  and  $\Psi'$  from data taken at different times with different running conditions was determined by superimposing Monte Carlo  $J/\Psi$  and  $\Psi'$  on real dimuon triggers from the different periods of the run. These efficiencies have been applied bin by bin to the  $J/\Psi$  and  $\Psi'$   $x_F$  and  $p_T$  distributions so that the data has been corrected for effects due to rate and spill structure variations. The global systematic uncertainty in the absolute level of the  $d\sigma/dx_F$  cross sections (and the differential cross sections,  $d\sigma/dp_T$  given in Table V) is 11.1%, 9.5%, 10.1% and 9.3% for the  $\pi$ ,  $\pi^+$ , proton and antiproton data, respectively, due to uncertainties in beam normalization, muon counter efficiencies and  $J/\Psi \rightarrow \mu\mu$  branching fraction which is known with a 3.9% error.



We have fit these data to two forms commonly used by other experiments for purposes of comparison. The first form is the empirical shape :

$$\frac{d\sigma}{dx_F} \propto (1 - |x_F - x_0|)^c \quad (1)$$

The second form is

$$\frac{d\sigma}{dx_F} \propto \frac{(1-x_1)^{n_1} (1-x_2)^{n_2}}{x_1 + x_2} \quad (2)$$

where  $x_1 = (x^* + x_F)/2$ ,  $x_2 = (x^* - x_F)/2$  and  $x^* = \sqrt{x_F^2 + 4m_\Psi^2/s}$

Parameterization (2) is inspired by the anticipated structure function factorization of the parton fusion process for the  $J/\Psi$  hadroproduction. If all  $J/\Psi$ 's are produced directly without processes based on color evaporation or  $\Psi'$  and  $\chi$  production and decay into  $J/\Psi$  being present<sup>8</sup>, each factor of  $(1 - x_m)^n$  would correspond to the structure function  $xF(x)$  for either the target or beam parton participating in the production process.

Fitting these forms to the differential cross sections of Fig. 6, we obtain the values of  $n_1$ ,  $n_2$ ,  $x_0$ , and  $c$  given in Table IV. The fit of parameterization (2) is shown superimposed on the data in Fig. 6.

Table IV  
Feynman x Differential Cross Section Fit Parameters

Beam	$n_1$	$n_2$	$x_0$	$c$
$\pi^+$	$1.81 \pm 0.16$	4.8 (fixed)	$0.030 \pm 0.013$	$1.99 \pm 0.15$
$\pi^-$	$1.90 \pm 0.14$	4.8 (fixed)	$0.062 \pm 0.011$	$2.27 \pm 0.27$
proton	$4.8 \pm 0.3$	$n_1 = n_2$	$0.026 \pm 0.007$	$4.14 \pm 0.16$
antiproton	$2.9 \pm 2.1$	$n_1 = n_2$	$-0.02 \pm 0.10$	$3.2 \pm 1.4$

We have used the parameters from the fit to the empirical form (1) to compare our  $x_F$  distributions to those obtained by other experiments. A parameterization of the world data performed by the E672 collaboration<sup>9</sup> using data from experiments over a wide range of energies and very different target and experimental configurations results in values of the exponent  $c$  at 300 GeV/c of  $2.9 \pm 0.14$  and  $4.7 \pm 1.6$  for the  $\pi^-$  and proton reactions to be compared with our results of  $2.22 \pm 0.27$  and  $4.14 \pm 0.16$ . However, more to the point, a direct comparison of our values of  $c$  with experiments in a similar energy range shows a very good agreement between our proton result

and the results of the E331, E444 and CS collaborations (as listed in Ref. 5), while the our pion result is in good agreement with WA11, and within two standard deviations of E331 and E444.

We have also fit our data to expression (2) to extract information about the gluon interactions resulting in  $J/\psi$  production. We have taken advantage of the approximate symmetry between the beam and target partons in the case of the proton beam by setting  $n_1=n_2$  in our fit of the proton data. This symmetry is strictly true for a natural Li target only if processes involving gluons dominate the  $J/\psi$  production processes and if the gluon distributions in a Li nucleon is not significantly modified by the presence of the other Li nucleons. If this approximation is good, the same symmetry can be used for the antiproton interactions since, by the CPT theorem, the gluon distribution for the antiproton must be the same as that of the proton. Furthermore, we have fixed the parton distribution in the target nucleons to that determined in the fits to our proton data when fitting our  $\pi^\pm$  data in order to lower the error on  $n_1$  for pions. The results of these fits are superimposed on the data of Fig. 6.

Assuming that two gluon fusion dominates the production of  $J/\psi$  as suggested by the near equality of the  $J/\psi$  production by proton and antiproton (see Table I), the Feynman  $x$  distribution for pN interactions can be predicted using the gluon structure functions of Duke and Owens<sup>10</sup>. Fitting the predicted  $d\sigma/dx_F$  distribution to expression (2) while holding  $n_1=n_2$ , we obtain  $n=3.8\pm0.04$  and  $1.90\pm0.04$  for Duke-Owens Set I and II respectively. However, this simple model cannot be correct by parity conservation. The two gluons must either fuse to form a  $\chi$  state which subsequently decays into  $\gamma\psi$  or must radiate a gluon. In either case according to the prescription of Kartvelishvili and Likoded<sup>11</sup> this will raise the exponent of the gluon distributions by approximately 1 unit to 4.8 and 2.9 respectively for the two Duke-Owens structure function sets. Assuming this prescription is correct, the measured value of  $4.8\pm0.3$  favors Duke-Owens Set I.

If we assume that the gluons also dominate the  $\pi^\pm$  production cross sections, the smaller values of the measured exponents ( $1.81\pm0.14$  and  $1.90\pm0.14$ ) shown in Table IV suggest a much stiffer momentum spectrum for the gluons in agreement with the naive picture of the pion in which a quark or gluon is expected to carry more momentum on average, although the situation is confused by the possible presence of quark-antiquark annihilation which can proceed without gluon radiation (thereby tending to lower the exponent).

Finally, we show the ratios of the differential cross sections for  $\pi^-$  to the  $\pi^+$  and for the composite  $\pi^\pm$  to the proton in Fig. 7 a and b respectively. Because of the Fermilab 800 GeV/c primary proton beam and the resulting large  $\pi^+$  fraction in the 300 GeV/c positive secondary beam, this experiment was capable of better comparisons of  $\pi^+$  and  $\pi^-$  interactions than previous experiments. As can be seen, the  $\pi^-/\pi^+$  ratio is independent of  $x_F$  and is approximately unity as expected. The ratio  $\pi^\pm/p$  on the other hand shows a significant increase at high  $x_F$  indicating a

harder gluon distribution of the pions and/or the onset of  $q\bar{q}$  processes.

The  $J/\psi$  differential cross sections as a function of transverse momentum ( $p_T$ ) for the four beam types are shown in Fig. 8a,b,c and d and tabulated in Table V.

Table V  
 $d\sigma/dp_T$  for  $J/\psi$  Production in 300 GeV/c  $\pi^\pm$ , Proton and Antiproton Interactions

$p_T$ (GeV/c)	$\pi^-$ (nb/GeV/c)	$\pi^+$ (nb/GeV/c)	$\bar{p}$ (nb/GeV/c)
0.125	81±4	59±6	52±4
0.375	183±6	177±9	138±7
0.625	239±7	229±11	178±9
0.875	235±7	233±11	181±7
1.125	209±7	210±10	158±8
1.375	161±6	152±9	118±7
1.625	121±5	128±8	78±6
1.875	79±4	61±6	55±4
2.125	52±3	36±4	30±3
2.375	25±3	23±4	13±3
2.625	14±2	15±3	4.5±1.6
2.875	8.5±1.4	5.3±2.3	1.4±0.9
3.125	3.5±1.0	3.2±2.1	0.82±0.65
3.375	1.6±0.9	2.0±1.9	0.60±0.60

$p_T$ (GeV/c)	$\bar{p}$ (nb/GeV/c)
0.25	116±62
0.75	180±46
1.25	134±36
1.75	77±24
2.25	30±21
2.75	7.4±11

The bin width is 0.25 GeV/c for the  $\pi^\pm$  and proton data and 0.5 GeV/c for the antiproton data. The errors associated with each cross section value are statistical. The systematic errors in the absolute level of these cross sections are the same as those quoted above for the  $d\sigma/dx_F$  differential cross sections.

We have fit these differential cross sections to

$$\frac{d\sigma}{dp_T^2} \approx e^{-p_T^2/p_0^2} \quad (3)$$

Using this form, the mean transverse momentum is  $\sqrt{\pi} p_0/2$  and the mean square of the transverse momentum is  $p_0^2$ . The values of the mean and the mean square of the transverse momentum are given in Table VI and the fits are shown superimposed on the data. The first error is the statistical error of the fit and the second is due to the rescaling of the muon momenta to fix the  $J/\psi$  mass at the world average.

Table VI  
 $\langle p_T \rangle$  and  $\langle p_T^2 \rangle$  of  $J/\psi$  Production in 300 GeV/c  
 $\pi^\pm$ , Proton and Antiproton Interactions

Beam	$\langle p_T \rangle$ (GeV/c)	$\langle p_T^2 \rangle$ (GeV <sup>2</sup> /c <sup>2</sup> )
$\pi^-$	$1.062 \pm 0.008 \pm 0.003$	$1.43 \pm 0.02 \pm 0.008$
$\pi^+$	$1.045 \pm 0.012 \pm 0.003$	$1.39 \pm 0.03 \pm 0.008$
proton	$0.993 \pm 0.002 \pm 0.003$	$1.255 \pm 0.005 \pm 0.008$
antiproton	$1.08 \pm 0.11 \pm 0.003$	$1.5 \pm 0.3 \pm 0.008$

In the case of the  $\pi^\pm$  data the assumed form of the differential cross section fails to fit the high  $p_T$  tail of the distributions while for the proton data and antiproton data the assumed shape of the  $p_T$  distribution is a good representation. Fig. 9a and 9b show the ratio of the  $p_T$  distributions for the  $\pi^-$  to  $\pi^+$  data and the composite  $\pi$  to proton data. As expected the  $\pi^-$  data is consistent with the  $\pi^+$  data with a ratio flat and consistent with unity in the range from 0 to 3 GeV/c. The  $\pi$  to proton ratio on the other hand is greater than 1 over the same range and increases with increasing  $p_T$ .

In summary, we have measured the total cross sections for  $J/\psi$  and  $\psi'$  hadroproduction by  $\pi^\pm$ , proton, and antiproton beams in Li interactions at 300 GeV/c. We have also measured the differential cross sections in  $x_F$  and  $p_T$  for  $J/\psi$  production. Several general conclusions can be drawn from the data. We find that the antiproton-nucleon cross section is not substantially larger than the proton-nucleon cross section for  $J/\psi$  production, suggesting that gluon fusion is the dominant mechanism for  $J/\psi$  production at these energies. In addition, the  $\pi^\pm$ -nucleon cross sections are very nearly equal implying that the production of  $J/\psi$  is due to a QCD process in contrast to an electromagnetic process. Comparing the  $\pi^\pm$ -nucleon cross sections with either the proton or antiproton cross sections, we see that the pion induced production of  $J/\psi$  is larger by approximately 25% than the  $p^\pm N$  cross section. This could be due to either the presence of valence

antiquarks in the  $\pi^\pm$  or to a large fraction of the pion momentum vested in the gluons. The large  $x_F$  enhancement of the  $d\sigma/dx_F$  distribution for pion induced production with respect to the proton induced production of  $J/\psi$  also suggests that the either quark-antiquark reactions become more important at high  $x_F$  or that the momentum of the gluons in the  $\pi^\pm$  is larger than in the nucleon. The larger high  $p_T$  tail of the  $d\sigma/dp_T$  for the  $\pi^\pm$  also seems to suggest a larger average parton momentum in the pion than in the proton.

We wish to thank the U.S. Department of Energy, the Natural Sciences and Engineering Research Council of Canada, the Quebec Department of Education, and the Scientific Affairs Division of the North Atlantic Treaty Organization for their support of this experiment. In particular, we wish to acknowledge the administration and staff of the Fermi National Accelerator Laboratory for their help.

## References

- <sup>1</sup>"The Experiment 705 Spectrometer: A Large Aperture Spectrometer at Fermilab to Study High Mass Dimuons and High Transverse Momentum Photons", L. Antoniazzi et al., submitted to Nucl. Inst. and Methods.
- <sup>2</sup>"The Experiment E705 Electromagnetic Calorimeter", L. Antoniazzi et al., submitted to Nucl. Inst. and Methods.
- <sup>3</sup>H. Areti et al., Nucl. Inst. and Meth. **212**, 135(1983)
- <sup>4</sup>D. Coffman et al., "A Direct Measurement of the  $J/\psi$  Leptonic Branching Fraction", SLAC-PUB-5592, (1991).
- <sup>5</sup>S.Katsanevas et al., E537 Collaboration, Phys. Rev. Lett. **60**, 2121(1988); J. Baider et al., NA3 Collaboration, Z. Phys. **C20**, 101(1983); K. Anderson et al., E444 Collaboration, Phys. Rev. Lett. **42**, 944(1979); J.G. Branson et al., E331 Collaboration, Phys. Rev. Lett. **38**, 1331(1977); C. Morel et al., UA6 Collaboration, CERN-PPE/90-127, (1990); E.J. Siskind et al., CS Collaboration, Phys. Rev. **D21**, 628(1980); E672 Collaboration, Fermilab-Pub-90-127, (1990) M. Abolins et al., WA11 Collaboration, Phys. Lett. **82B**, 145(1979).
- <sup>6</sup>L. Lyons, Prog. Part. Nucl. Phys. **7**, 169(1981).
- <sup>7</sup>M.J. Corden et al., Omega Collaboration, Phys. Rev. Lett. **B96**, 411(1980); S. Katsanevas et al., E537 Collaboration, Phys. Rev. Lett. **60**, 2121(1988); J.G. Branson et al., E331 Collaboration, Phys. Rev. Lett. **38**, 1331(1977); K. Anderson et al., E444 Collaboration, Phys. Rev. Lett. **42**, 944(1979); H.D. Snyder et al., E288 Collaboration, Phys. Rev. Lett. **36**, 1415(1979); A.G. Clark et al., Nucl. Phys. **B142**, 29(1978); UA1 Collaboration, CERN-PPE/90-154, (1990).
- <sup>8</sup>"Production of  $J/\psi$  via  $\psi'$  and Radiative  $\chi$  Decay in 300 GeV/c Proton and  $\pi^\pm$  Interactions", L. Antoniazzi et al., submitted to Physical Review Letters.
- <sup>9</sup>V. Abramov et al., E672/706 Collaboration, Fermilab-Pub-91/62-E, (1991).
- <sup>10</sup>D.W. Duke and J.F. Owens, Phys. Rev. **30D**, 49(1984).
- <sup>11</sup>V.Kartvelishvili and A.K. Likoded, Sov. J. Nucl. Phys. **39**, 298(1984).

## Figure Captions

Fig. 1 Fermilab High Intensity Laboratory Beam Transport System

Fig. 2 E705 Large Aperture, Open Geometry Spectrometer

Fig. 3 E705  $\mu^+\mu^-$  mass spectra for  $\pi^\pm$  and  $p^\pm$  Li Interactions at 300 GeV/c

Fig. 4  $BR(J/\psi \rightarrow \mu\mu) \cdot \sigma(x+N \rightarrow J/\psi + x')$  vs  $\sqrt{\tau}$  for a)  $\pi^+$ , b)  $\pi^-$ , c) proton and d) antiproton interactions

Fig. 5  $BR(\psi' \rightarrow \mu\mu) \cdot \sigma(x+N \rightarrow \psi' + x') / BR(J/\psi \rightarrow \mu\mu) \cdot \sigma(x+N \rightarrow J/\psi + x')$  vs  $\sqrt{\tau}$  for a)  $\pi^+$ , b)  $\pi^-$ , c) proton and d) antiproton interactions

Fig. 6  $d\sigma/dx_F$  differential cross sections for  $J/\psi$  hadroproduction in 300 GeV/c a)  $\pi^+$ , b)  $\pi^-$ , c) proton and d) antiproton interactions. The fits are to equation (2) given in text.

Fig. 7 Ratio of  $J/\psi$   $d\sigma/dx_F$  differential cross sections for a)  $\pi^+$  to  $\pi^-$  data sample, b)  $\pi$  to proton data sample.

Fig. 8  $d\sigma/dp_T$  for  $J/\psi$  hadroproduction in 300 GeV/c a)  $\pi^-$ , b)  $\pi^+$ , c) proton and d) antiproton interactions. The curves are fits to equation (3) of the text.

Fig. 9 Ratio of  $J/\psi$   $d\sigma/dp_T$  differential cross sections for a)  $\pi^-$  to  $\pi^+$  data sample, b)  $\pi$  to proton data sample.

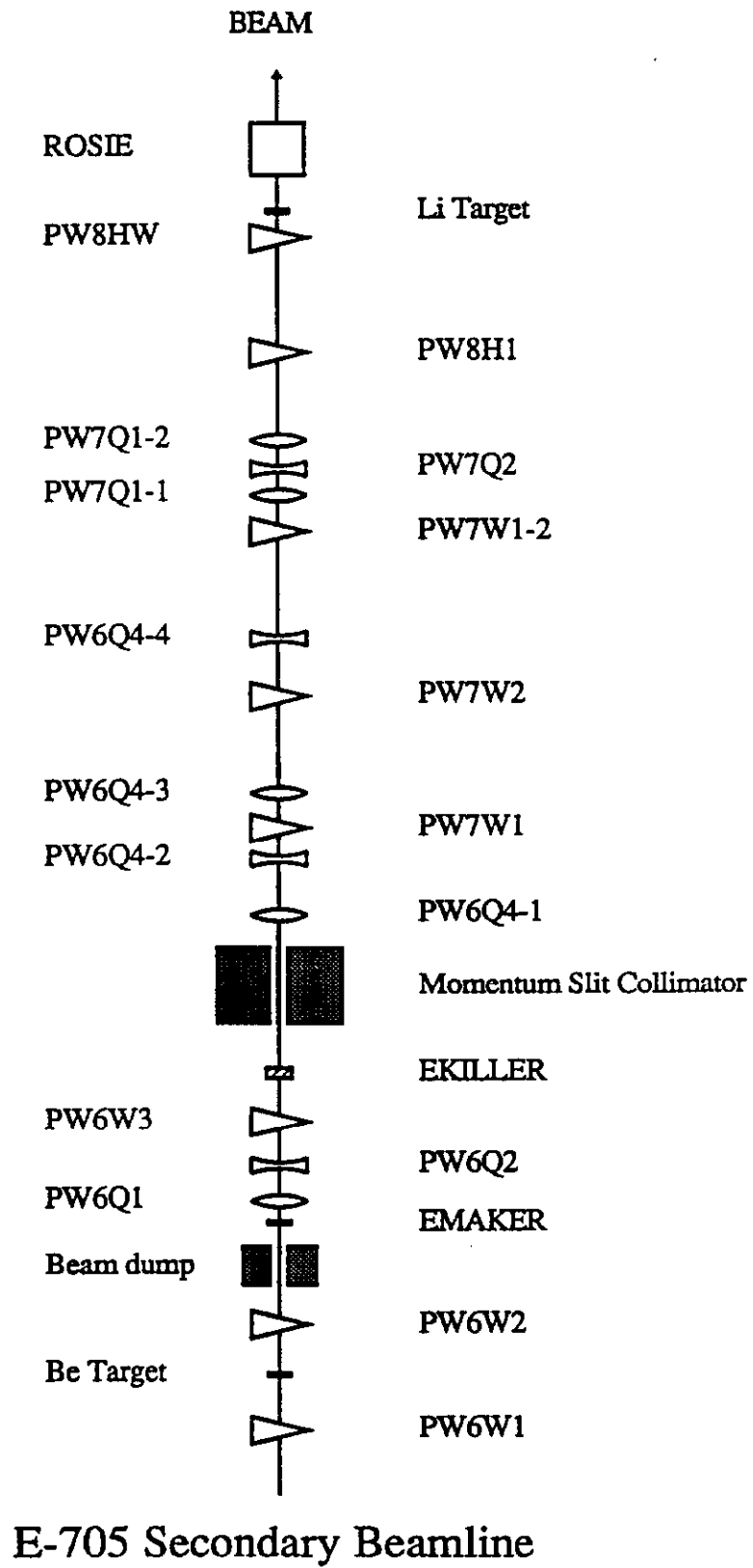


Fig. 1



# FERMILAB HIGH INTENSITY LAB SPECTROMETER E705

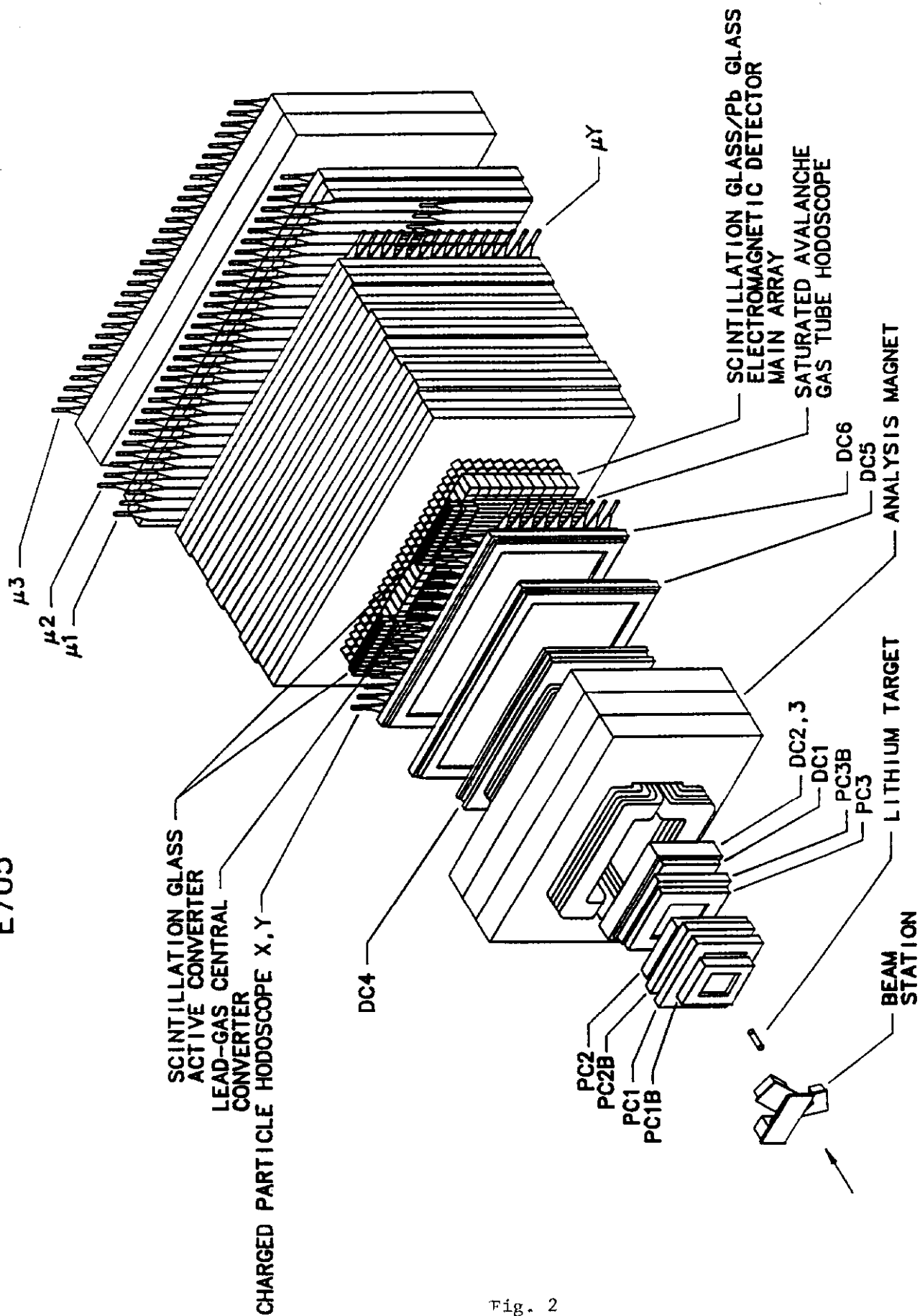


Fig. 2

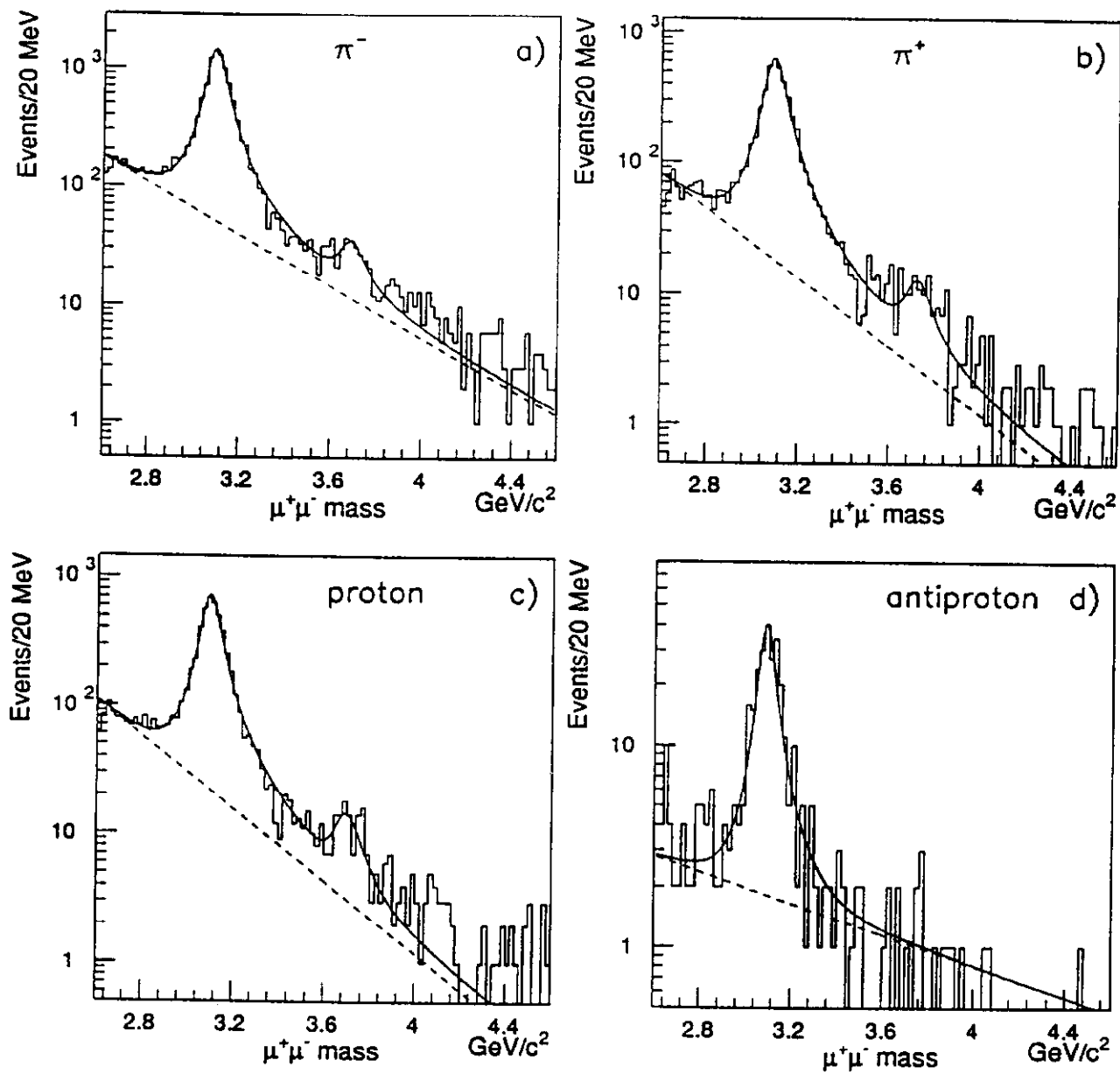
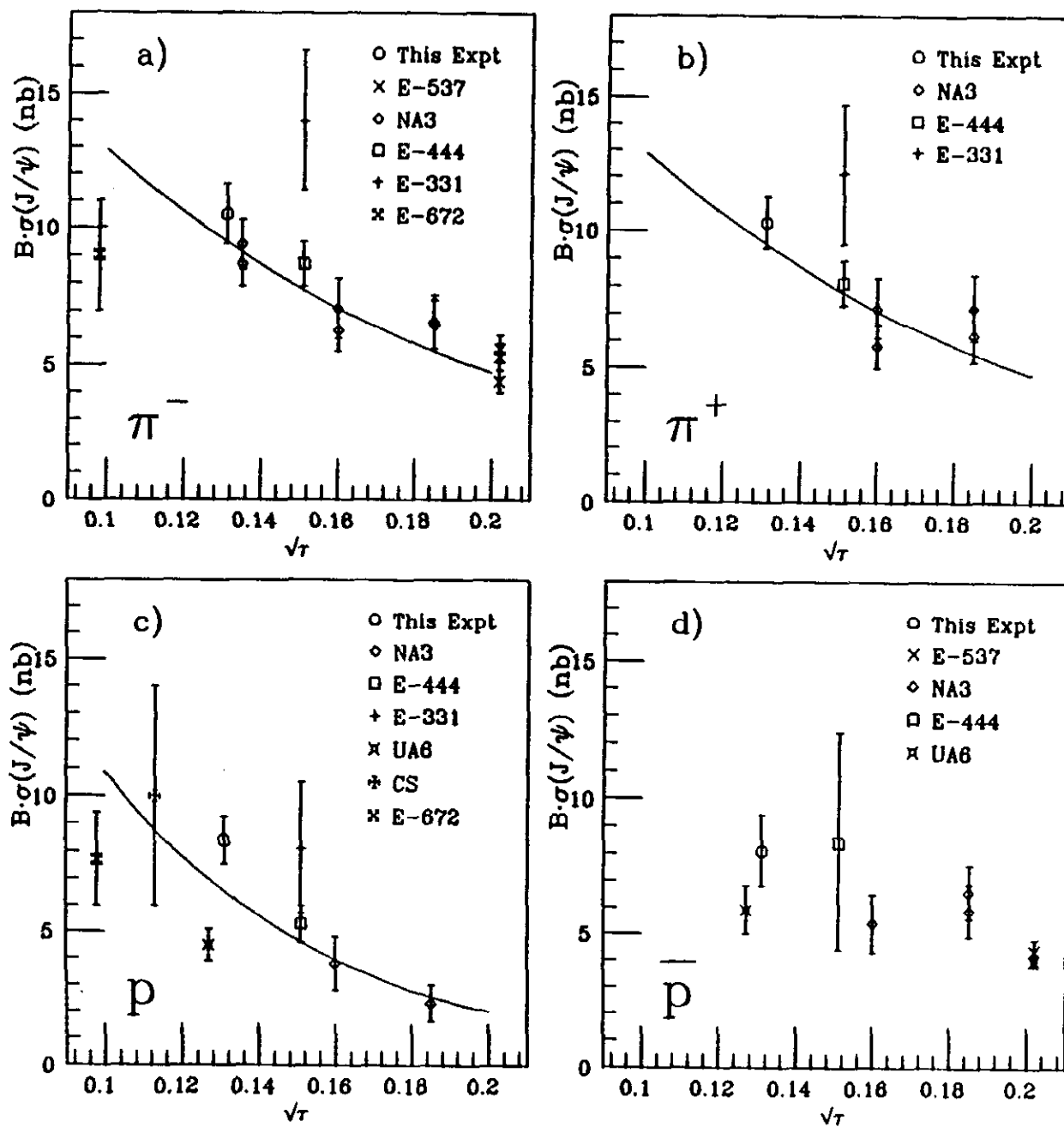


Fig. 3



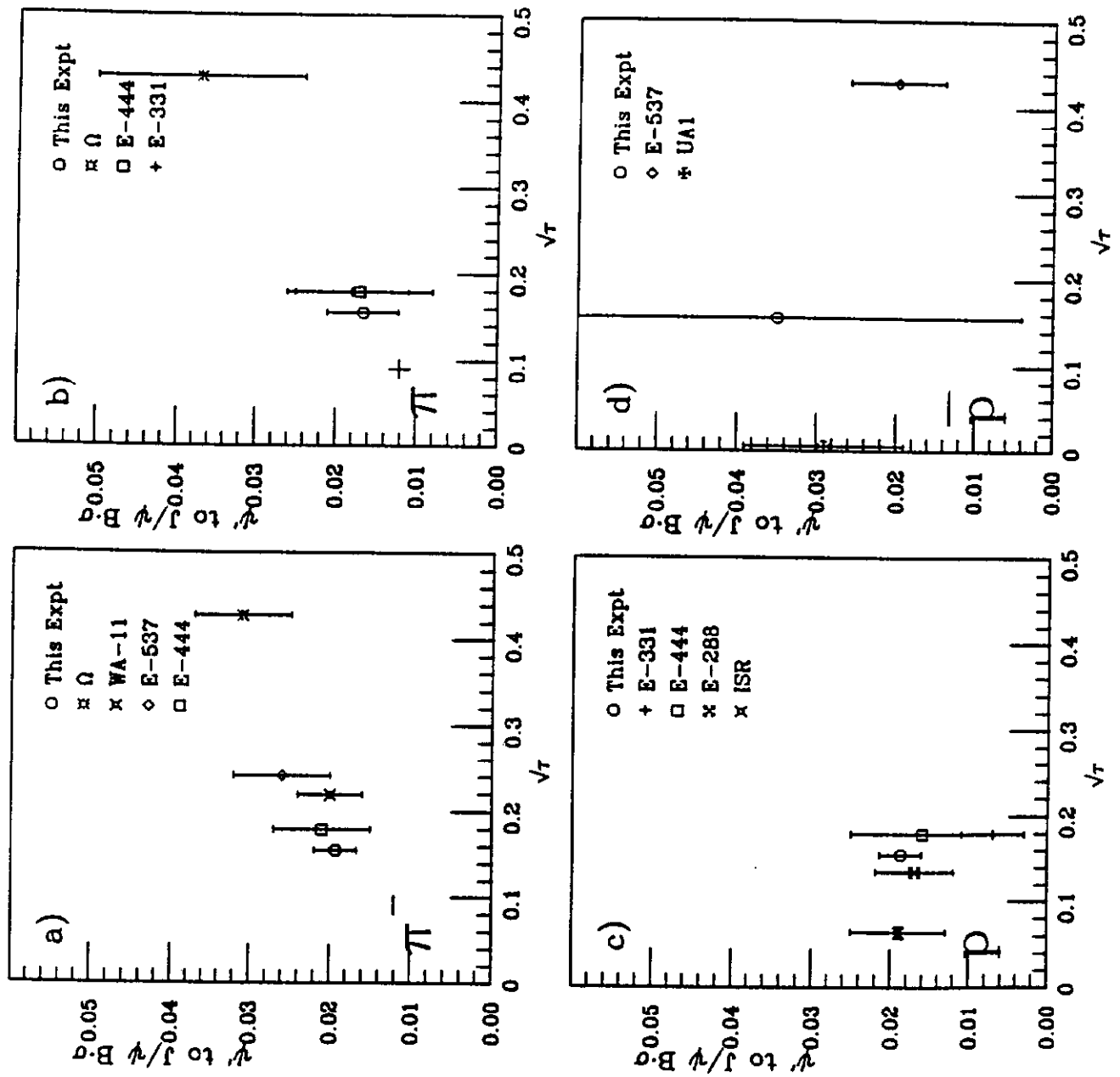


Fig. 5

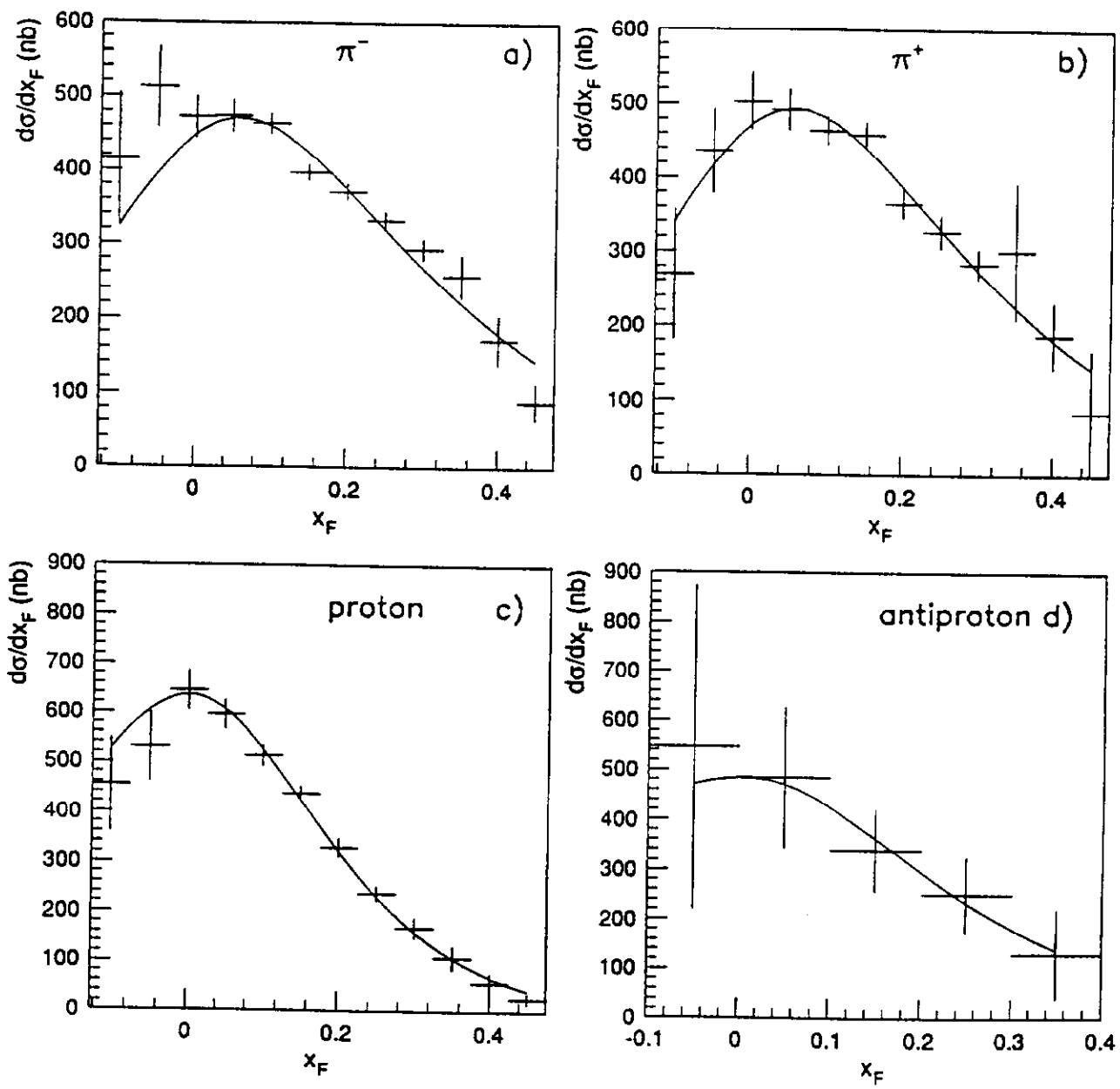


Fig. 6

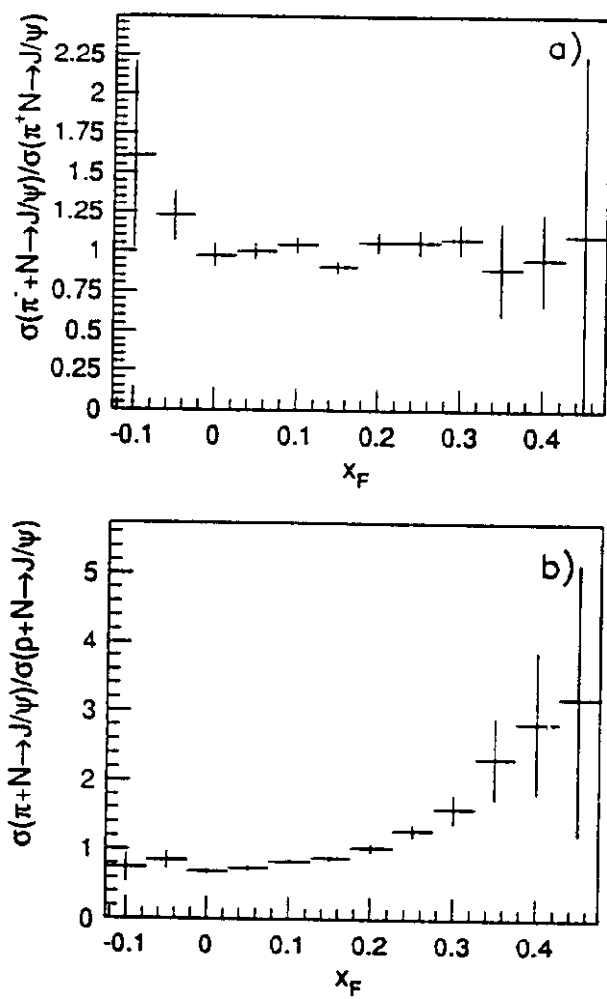


Fig. 7

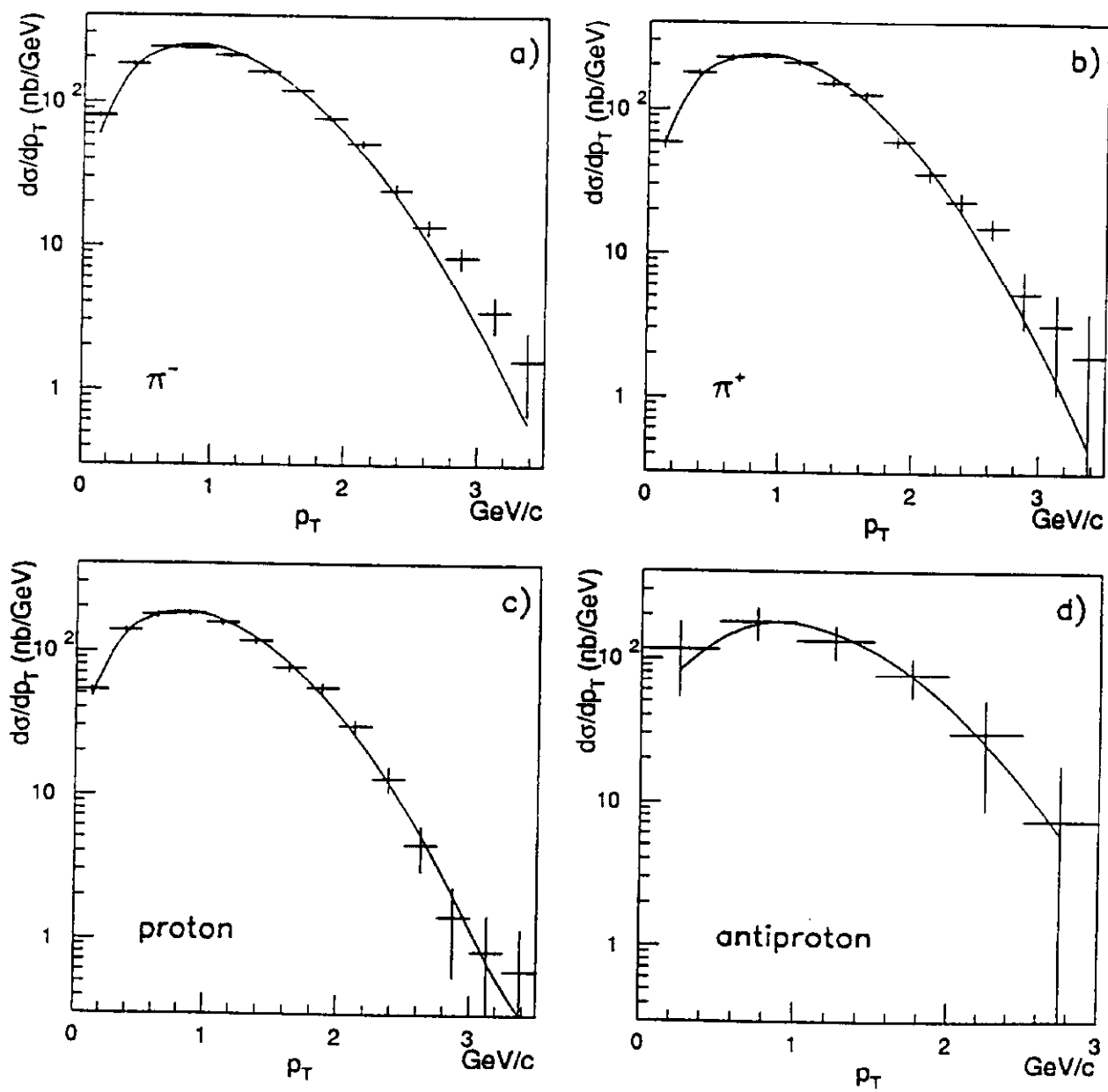


Fig. 8

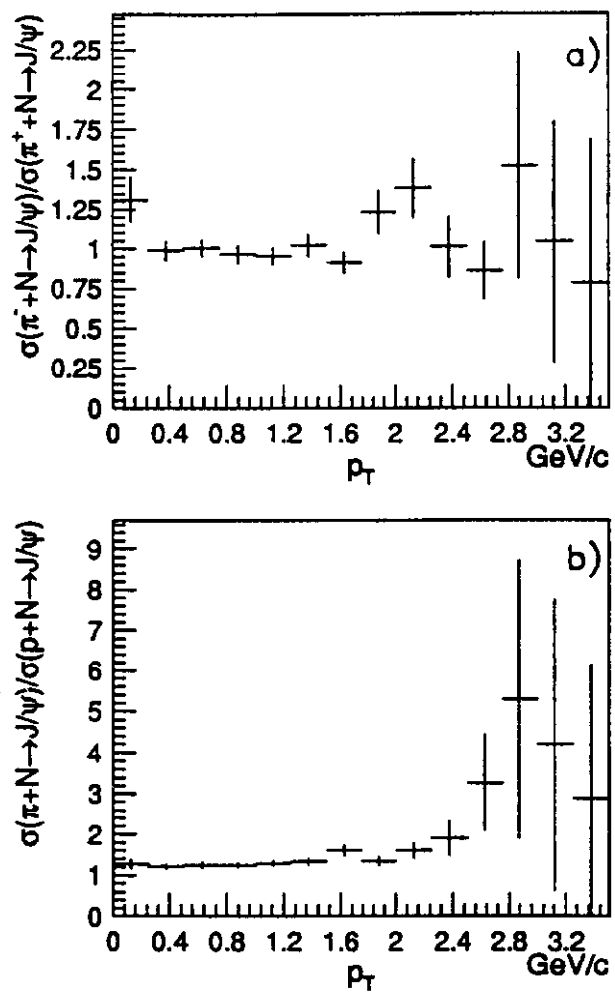


Fig. 9